Journal of Renewable Materials

Tech Science Press

DOI: 10.32604/jrm.2024.055122

ARTICLE

# Mechanical Behavior of Panels Reinforced with Orthogonal Plant Fabrics: Experimental and Numerical Assessment

**Martha L. Sánchez[1,*] and G. Capote[2]**

[1]Universidad Militar Nueva Granada, Programa de Ingeniería Civil, Bogotá, 110111, Colombia

[2]Facultad de Ciencias, Departamento de Física, Universidad Nacional de Colombia, Bogotá, 111321, Colombia

[*]Corresponding Author: Martha L. Sánchez. Email: martha.sanchez@unimilitar.edu.co

Received: 18 June 2024 Accepted: 13 August 2024 Published: 23 October 2024

## ABSTRACT

The construction sector is one of the main sources of pollution, due to high energy consumption and the toxic substances generated during the processing and use of traditional materials. The production of cement, steel, and other conventional materials impacts both ecosystems and human health, increasing the demand for ecological and biodegradable alternatives. In this paper, we analyze the properties of panels made from a combination of plant fibers and castor oil resin, analyzing the viability of their use as construction material. For the research, orthogonal fabrics made with waste plant fibers supplied by a company that deals with the manufacture of furniture and craft products were used. These fabrics were made with strips of plant fibers of the *Calamus rotang*, *Bambusa vulgaris*, *Heteropsis flexuosa*, and *Salix viminalis* species. To improve their compatibility with the castor oil resin, a cold argon plasma treatment was applied. The effect of the treatment on the properties of the fibers and the panels was analyzed. The density, water absorption capacity, and swelling percentage were evaluated. Tensile, compression, static bending, and linear buckling tests were carried out. The study found that panels made with treated fiber fabrics exhibited a reduction of approximately 10% in absorption capacity and up to 35% in swelling percentage values. Panels made with *Bambusa vulgaris* fabrics exhibited the highest strength and stiffness values. Numerical models were constructed using commercial finite element software. When comparing the numerical results with the experimental ones, differences of less than 15% were seen, demonstrating that the models allow adequately predicting the analyzed properties. On comparing the values obtained with the characteristic values of oriented strand board, the results suggest that panels made with unconventional materials could replace commercial panels traditionally made with wood-based fibers and particles and other composite materials in several applications in the construction industry.

## KEYWORDS

Unconventional materials; nonstructural panels; plant fibers; surface treatment; physical properties; mechanical properties

## Nomenclature

| | |
|---|---|
| A | Absorption |
| CI | Crystallinity index |
| d | Fiber diameter |

| | |
|---|---|
| D | Density |
| $D_w$ | Density of weave |
| $E_c$ | Modulus of elasticity in compression |
| $E_t$ | Modulus of elasticity in tension |
| FWHM 1 | Full Width at Half Maximum |
| H | Intensity |
| K | Shape factor |
| L | Crystallite length |
| MOE | Apparent modulus of elasticity |
| MOR | Modulus of rupture |
| NT | Untreated fibers |
| NT-BF-P | Panels made with untreated *Bambusa vulgaris* fibers |
| NT-HF-P | Panels made with untreated *Heteropsis flexuosa* fibers |
| NT-RF-P | Panels made with untreated *Calamus rotang* fibers |
| NT-SF-P | Panels made with untreated *Salix viminalis* fibers |
| Pcr | Critical linear buckling load |
| Sw | Swelling percentage |
| TR | Treated fibers |
| TR-BF-P | Panels made with treated *Bambusa vulgaris* fibers |
| TR-HF-P | Panels made with treated *Heteropsis flexuosa* fibers |
| TR-RF-P | Panels made with treated *Calamus rotang* fibers |
| TR-SF-P | Panels made with treated *Salix viminalis* fibers |
| $x_c$ | Diffraction angle |
| $\varepsilon$ | Strain percentage |
| $\sigma_c$ | Compression strength |
| $\sigma_t$ | Tensile strength |
| $2\theta$ | Diffraction angle |

## 1 Introduction

The construction industry has a major impact on the environment, since it represents a significant percentage of total resource consumption, energy use, and greenhouse gas emissions. One of the indicators used to evaluate the environmental impact generated by the construction industry is the consumption of materials throughout the life cycle of buildings. Understanding material consumption helps identify opportunities for efficient use of resources, promoting circular economy principles and developing more sustainable materials practices [1,2].

According to Zimmer et al., Latin America affords a wide availability of natural resources that promote the production and use of conventional fiber or wood particle boards in various non-structural applications in the construction sector [3]. However, it is important to consider that timber extraction can lead to deforestation and loss of biodiversity if not managed sustainably. On the other hand, although these fibers come from renewable resources, synthetic adhesives (urea formaldehyde, melamine urea formaldehyde, phenol formaldehyde, etc.) are frequently used during the manufacture of these boards. These resins cause polluting emissions, causing damage to human health [3].

Recent research has focused on the study of sustainable materials that can be used to replace petrochemical polyols used as resins to produce fiber or particle boards. Several vegetable oils (castor oil,

soybean oil, palm oil, linseed oil, etc.) have been evaluated with the aim of reducing the environmental impact and energy consumption generated by traditional polyurethanes. In recent years, studies have been carried out promoting the development of castor oil-based polyurethanes for adhesive applications on wood and other plant fibers [4–7].

The use of unconventional plant fibers such as flax, kenaf, linen, palm, and cassava as substitutes for traditional fibers in the production of non-structural panels is gaining increasing attention [8–12]. The development and application of these panels can contribute to the mitigation of the environmental footprint generated when using conventional construction materials and has stimulated the spread of the use of more ecological materials containing plant-based fibers [13], which are distinguished for their notable physical and mechanical properties, such as a high degree of strength, stiffness, toughness, thermal insulation, and cost-effectiveness [14].

The mechanical properties of composites reinforced with plant fibers vary depending on determining factors such as the selection of the type of reinforcement, the fiber load, and their compatibility with the matrix of the composites [14]. Recent studies have shown that the combination of different types of fibers as reinforcement of polymeric matrix can contribute to improving the mechanical properties of composites. Some of these studies have focused on evaluating the effect of the stacking sequence on the mechanical behavior of flax/carbon/kevlar based epoxy, jute/hemp bio-epoxy, and flax/basalt/carbon fiber reinforced epoxy/bio epoxy hybrid composites. The results favor the use of hybrid composites in various structural engineering applications [15–17].

Despite their multiple advantages, some factors, such as the hydrophilicity of vegetal fibers and their polysaccharide content, may limit their use as reinforcement in panels made with biopolymeric resins [13,14]. According to Vinod et al., the hydrophilic nature of natural fibers can be reduced by means of chemical treatment and surface modification techniques [18]. These treatments allow for the partial elimination of lignin, hemicellulose, wax, and some impurities, which can affect their adhesion to the composite matrix [19,20]. Currently, physical modification methods have been applied, with novel results for the surface modification of fibers [21]. These methods are considered “clean methods” because their application does not generate polluting residues. Cold plasma treatments using methane, argon, or helium are the most employed physical processes. This technique generates free radicals and polymerizes the material, modifying the chemical structure of the fibers and their crystallinity index [22]. Recent results have shown the effect of surface modifications on the behavior of composite panels made with materials of plant origin, emphasizing the materials’ performance when subjected to axial and bending loads [23].

Due to their physical and mechanical properties, panels made from plant-based fibers and resins could be used in various non-structural applications. In general, during its useful life, the material can be subjected to the action of external loads that can affect its durability and mechanical performance. Recent studies have reported experimental and numerical results focused on an analysis of composites subjected to various loading conditions, analyzing the viability of their use in several sectors of industry [24]. Pathak et al. evaluated the buckling behavior of composite plates under combined mechanical and thermal loading [25]. Jiao-Wang et al. studied the critical buckling load of slender flax/PLA columns subjected to uniaxial compression, comparing the numerical results with experimental tests in order to validate Ludwick’s law for predicting the critical buckling load of nonlinear elastic columns [26]. Gioffrè et al. analyzed the mechanical behavior of a hemp-based biocomposite material and its use as a structural reinforcement for masonry structures [27]. Jungstedt et al. compared hot-pressed lignocellulosic composites, examining the strains and failure mechanisms associated with these materials. Their results suggest that the application of hot-pressed all-lignocellulose composites could extend beyond packaging to include load-bearing applications, such as molded panels for buildings and transportation [28].

Additionally, Kan et al. proposed a strategy for adjusting cross-linking networks in soybean meal-based biocomposites, effectively balancing their mechanical and biodegradation properties [29].

In this paper, the physical and mechanical properties of non-conventional panels subjected to different loading conditions (tension, compression, static bending, and linear buckling) are presented. For the construction of the panels, orthogonal plant fabrics were used to reinforce a castor oil matrix. The fabrics were made using plant waste supplied by a company that deals in the manufacture of furniture and craft articles. To improve the compatibility between the plant fibers and the castor oil resin, a preliminary surface treatment using a cold argon plasma was applied. The experimental results were compared with the results obtained for commercial wood panels. Additionally, numerical models were developed that allow predicting the behavior of the material subjected to different loading conditions.

## 2 Experimental Procedures

### *2.1 Constituent Materials*

Vegetable fiber strips of the *Calamus rotang* (RF), *Bambusa vulgaris* (BF), *Heteropsis flexuosa* (HF), and *Salix viminalis* (SF) species were used. The fibers were supplied by a company that deals in the manufacture and marketing of furniture and craft products. The fibers used come from tropical plants widely available in South America. The availability, rapid growth, and physical and mechanical properties of these plant fibers make them a viable option for the actual production of a wide range of products in various industry sectors.

The content of cellulose, hemicellulose, lignin, and other compounds (oil, waxes, and impurities) was determined following the procedures described in ASTM D1103-21 [30], ASTM D1110-21 [31], and ASTM D1106-21 [32]. The chemical composition of the fibers is presented in Table 1. A commercial bicomponent castor oil resin based on vegetable polyurethane was used as the matrix of the panels. The resin consists of two components (A + B) mixed in a proportion of 1:1.5 (one part of component A and, one and a half parts of component B, in volume, respectively). Component A is a product obtained by pre-polymerization of diphenylmethane diisocyanate with polyol derived from castor oil. Component B is a product derived from castor oil, obtained by esterification and transesterification of ricinoleic acid with glycols. The properties of hardened castor oil resin were provided by the supplier and are presented in Table 2.

**Table 1:** Chemical composition of fibers

| Fibers | Cellulose (%) | Hemicellulose (%) | Lignin (%) | Others (%) |
|---|---|---|---|---|
| RF | 47 ± 4 | 23 ± 2 | 25 ± 4 | 5.0 ± 0.3 |
| BF | 49 ± 2 | 18 ± 3 | 25 ± 3 | 6.0 ± 0.2 |
| HF | 45 ± 3 | 20 ± 4 | 26 ± 2 | 9.0 ± 0.4 |
| SF | 46 ± 4 | 28 ± 3 | 17 ± 4 | 9.0 ± 0.5 |

**Table 2:** Properties of hardened castor oil resin

| | |
|---|---|
| Tensile strength (MPa) | 55 ± 5 |
| Modulus of elasticity (GPa) | 2.5 ± 0.3 |
| Poisson coefficient | 0.38 ± 0.04 |
| Density (kg/m$^3$) | 1025 ± 18 |

### *2.2 Surface Treatment and Fiber Characterization*

A cold argon plasma was applied using a plasma-enhanced chemical vapor deposition (pulsed-DC PECVD) system. This treatment is a dry modification process, in which no drying is required after the treatment step. At the same time, the consumption of chemical products is very low, which allows reducing the emission of polluting waste. The plasma was applied for 30 min at a working pressure of 120 Pa, with an applied voltage of −300 V and a temperature not exceeding 30°C. A Tescan Vega scanning electron microscope (SEM) was used to analyze potential changes in the morphology of the fibers. Micrographs with a magnification of 400× were obtained before and after the plasma treatment. To evaluate the influence of the treatment on the elemental composition of the fibers, the X-ray dispersion spectroscopy (EDS) technique was used.

The X-ray diffraction (XRD) technique was applied using a PANalytical XPert PRO MRD X-ray diffraction system. The crystallinity index was determined using the Segal method [33]. Fourier transform infrared spectroscopy (FTIR) was applied using a Thermo Scientific Nicolet iS10 with an ATR module with a measurement range between 600 and 4000 $cm^{-1}$ and 16 scans.

The density (D), water absorption capacity (A), swelling percentage (Sw), tensile strength ($\sigma_t$), modulus of elasticity ($E_t$), and strain percentage ($\varepsilon$) of the fibers were evaluated according to the procedures described in the ASTM D792-20 [34] and ASTM D3800-20 [35] standards, respectively. The diameter of individual fibers was measured using a Nikon SMZ800 stereo zoom microscope. Average values were reported by measuring the diameter of the fiber at 8 random places. 50 specimens were analyzed for each type of plant fiber.

### *2.3 Manufacturing Process*

#### *2.3.1 Fabrics*

A “hand-woven” fiber arrangement was used. The weave consisted of strips with a thickness of 2 mm, a width of 8 mm, and a length of 300 mm. In each fabric, the orientation of the strips was combined at 0° and 90°, forming a plain weave arrangement, which is characterized by its easy production, symmetry, and stability (see Fig. 1).

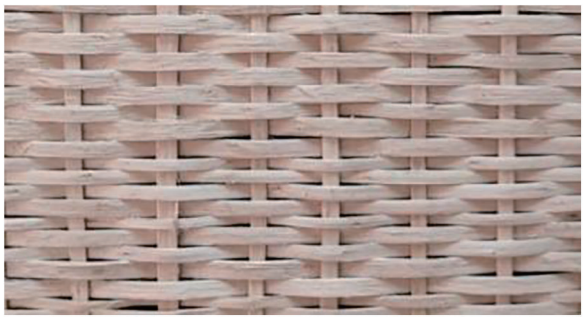

**Figure 1:** Plain weave arrangement

#### *2.3.2 Panels*

For the elaboration of the panels, the constituent materials were mixed in a proportion of 70% fibers and 30% resin, based on the total volume of the panel. Thin square panels measuring 300 mm in width, 300 mm in length, and 8 mm in thickness were constructed using the manual molding technique and compression compaction [36]. A hydraulic press with a card capacity of 1000 kN was used. A load of 100 kN at room temperature was applied for 6 h. Once removed from the mold, the panels were cured for 72 h.

To evaluate the efficiency of the argon plasma treatment, panels reinforced with untreated (NT) and treated (TR) fibers were manufactured for each type of vegetal fiber.

### *2.4 Panel Characterization*

The density (D), water absorption capacity (A), and swelling percentage (Sw) of the panels were determined following the recommendations of the ASTM D2395-17 [37] and ASTM D1037-20 [38] standards, respectively.

The tensile, compression, and static bending tests were performed following the procedures described in ASTM D1037-20 [38]. For the tests, a Landmark MTS 370.10 with load capacity of 100 kN was used. For the tensile test, specimens 254 mm long, 50.8 mm wide, and 8 mm thick were produced. A reduced section of width 38 mm was designed in the central region of the specimens. The tensile load was applied at a uniform rate of 4 mm/min. For the compression test, specimens of 50 mm in width, 8 mm in thickness, and 100 mm in length were evaluated. The load was applied at a uniform rate of 0.5 mm/min. To determine the modulus of rupture (MOR) and apparent modulus of elasticity (MOE), specimens 75 mm wide, 8 mm thick, and 250 mm long were used. The distance between supports was 200 mm, and the rate of application of load was 3 mm/min. Numerical models were developed using commercial finite element software. For the simulation, a linear static analysis and a mesh with S8R-type elements were employed.

For the buckling test, specimens 300 mm wide, 300 mm high, and 8 mm thick were evaluated. Displacement at a speed of 1 mm/min was applied. The critical linear buckling load (Pcr) was determined experimentally and compared with that obtained in the numerical model. In the models, a linear buckling perturbation was considered. To simulate compression loading, the application of a unitary load line across the entire upper edge of the panel was adopted. In this way, it was possible to obtain the size of the buckling load by multiplying the obtained eigenvalue by the width of the panel.

## 3 Results and Discussions

### *3.1 Effect of the Plasma Treatment on the Morphology of the Fibers*

SEM micrographs for untreated and treated fibers are presented in Figs. 2–5. In Figs. 2a, 3a, 4a, and 5a, the presence of impurities and non-cellulosic compounds adhered to the surface of the fibers can be seen. On comparing these figures, differences in the microstructural shapes of the fibers can be observed. In Figs. 2b, 3b, 4b, and 5b, a cleaner and more defined surface is shown.

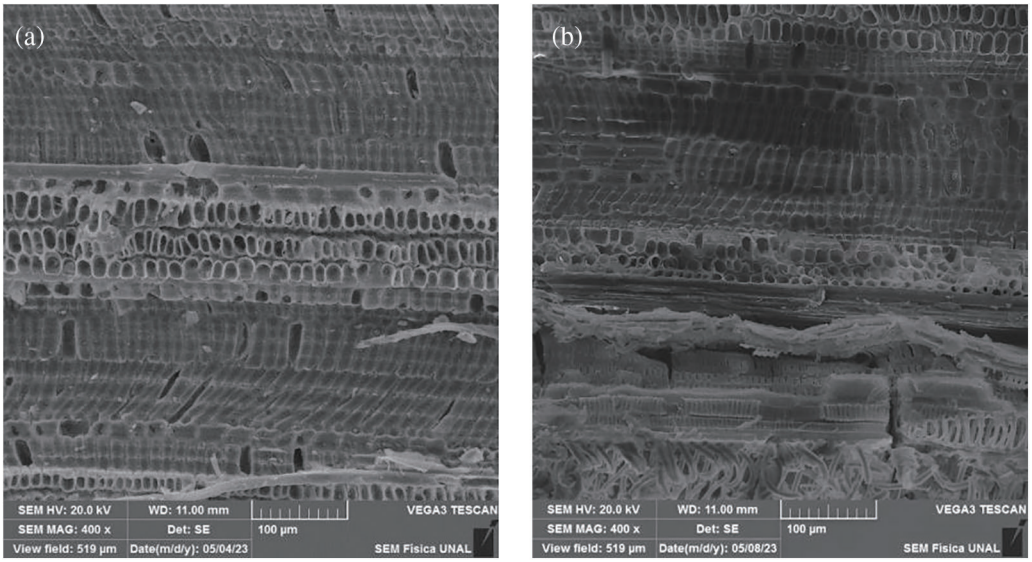


**Figure 2:** Effect of treatment on morphology of NT-RF (O/C = 0.91) (a) and TR-RF (O/C = 0.97) (b)

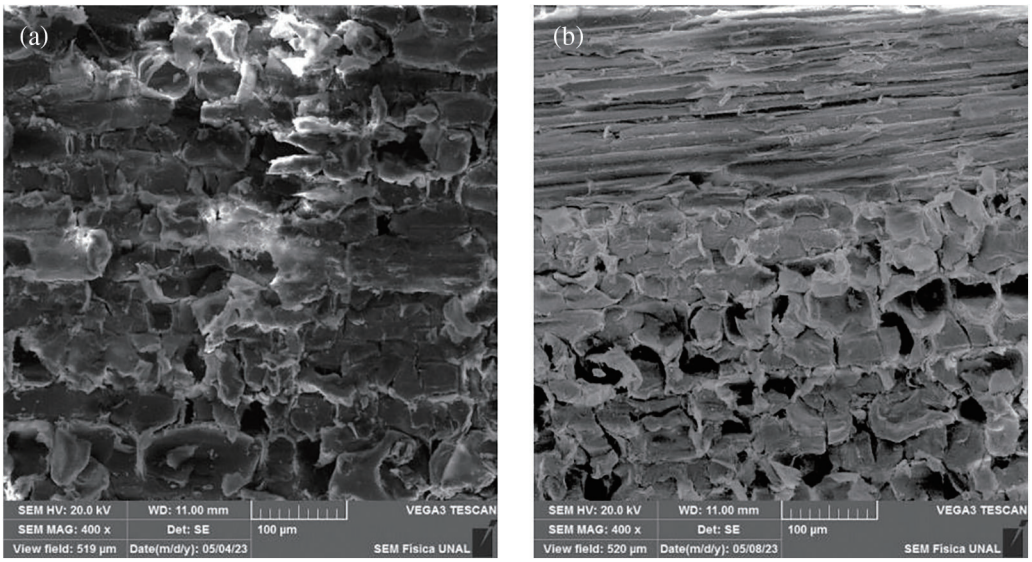


**Figure 3:** Effect of treatment on morphology of NT-BF (O/C = 0.80) (a) and TR-BF (O/C = 0.83) (b)

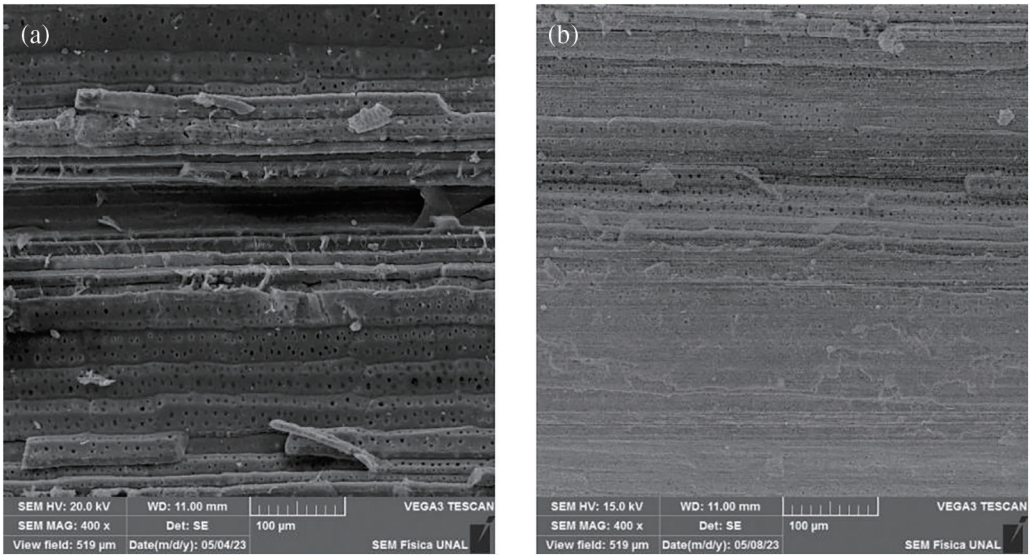


**Figure 4:** Effect of treatment on morphology of NT-HF (O/C = 0.82) (a) and TR-HF (O/C = 0.83) (b)

The appearance of microvoids and a fibrillar structure indicates the efficiency of the treatment for the removal of non-cellulosic compounds. Some modifications in the elemental composition of the fibers were observed using the EDS technique. The results indicate a nearly 7% increase in the oxygen/carbon (O/C) ratio of the TR-RF and TR-SF fibers. However, on analyzing the results for TR-BF and TR-HF, only a slight increase in the O/C ratio (less than 5%) can be seen. According to Sawangrat et al., argon treatment causes an increase in the surface activity of the fibers, favoring the reaction of free radicals with oxygen, reducing the atomic percentage of carbon and increasing the atomic percentage of oxygen [39]. Nevertheless, the effect of the treatment on the surface of the fibers may vary depending on the plant species, sometimes causing the degradation of any of its compounds.

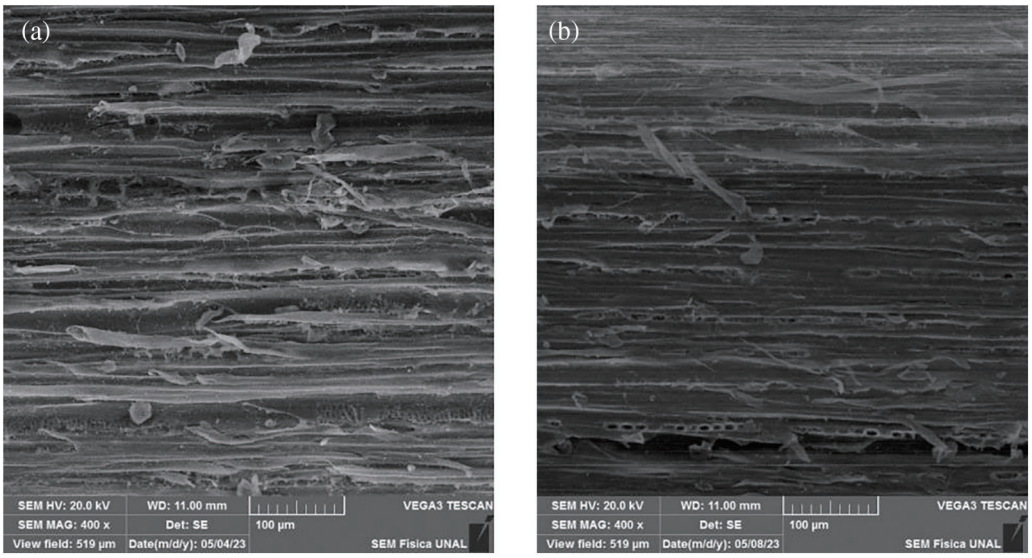


**Figure 5:** Effect of treatment on morphology of NT-SF (O/C = 0.86) (a) and TR-SF (O/C = 0.93) (b)

### *3.2 Effect of Treatments on the Chemical Properties of the Fibers*

The X-ray diffraction spectra of the fibers are presented in Fig. 6a. Peaks located nearest 14.80°, 16.50°, and 22° can be seen in Fig. 6b. The presence of these peaks corresponds to the crystallographic planes $1\bar{1}0$, 110 and 200, which denote the presence of cellulose 1β [40].

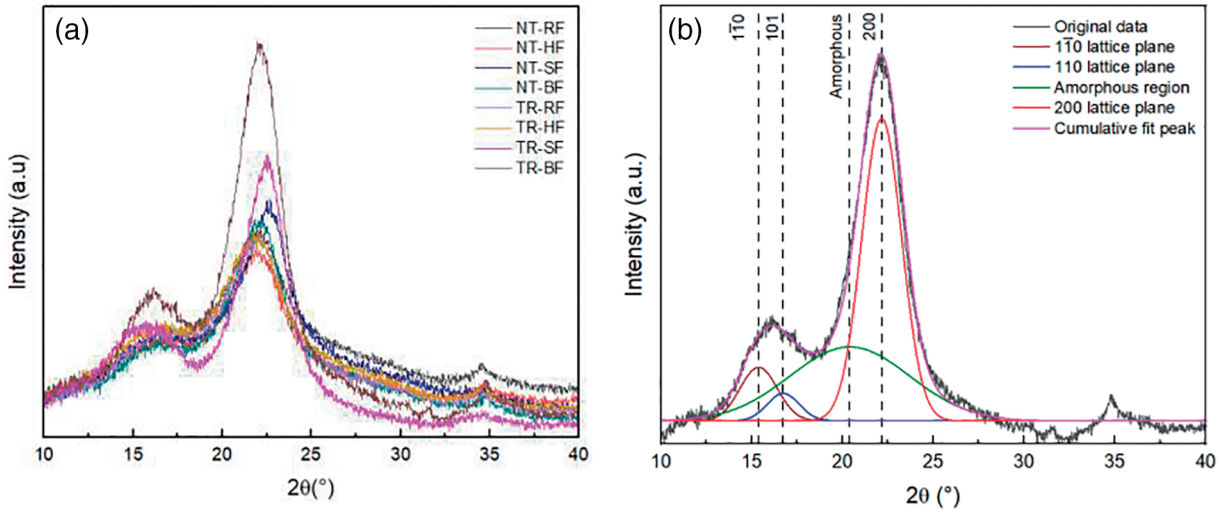


**Figure 6:** X-ray diffraction spectra (a); deconvolution and identification of crystallographic planes (b)

Using the Segal equation, the crystallinity index (CI) was calculated. Additionally, the size of the crystallite was determined using the Scherrer equation, considering a wavelength of 1.544426 and a shape factor of K = 0.9. Results are shown in Table 3.

From these results, it can be seen that the crystallinity index significantly increased in all treated fibers between 20% and 80%. Similar results were obtained by Sahu et al. when they analyzed the effect of various surface treatments on the crystallinity index and the crystallite size of Rattan fibers [41]. Analysis of the effect

of the surface treatment on the CI values is a complex process that depends on several factors, such as the morphology of plant species, the treatment conditions, the resistance to degradation, the size of the crystallite, and the presence of some defects in the crystalline structure. The increase in the CI values may be associated with the removal of non-cellulosic compounds (amorphous compounds) and the reorganization of the cellulose chains, each of which promotes a more ordered and compact structure, thus improving the crystallinity of the fibers [40]. On analyzing the effect of the treatment on the crystallite size (L), an increase of up to 18% was observed in the treated fibers. According to Vinod et. al., this increase in the size of the crystallite can affect some of the fibers' physical properties, such as absorption capacity, thus improving their performance as reinforcement for polymeric matrices [40].

**Table 3:** Crystallinity index and crystallite length obtained using deconvolution data

| Fibers | $x_c$ (°) | H (a.u.) | FWHM (°) | CI (%) | L (nm) |
|---|---|---|---|---|---|
| NT-RF | 14.35 | 240.54 | 1.94 | 40.95 | 4.59 |
| | 16.93 | 317.56 | 1.64 | | |
| | 21.15 | 1377.11 | 6.54 | | |
| | 22.10 | 2332.06 | 1.84 | | |
| TR-RF | 14.77 | 124.34 | 1.02 | 55.35 | 5.42 |
| | 16.87 | 472.34 | 1.87 | | |
| | 19.42 | 1231.00 | 6.71 | | |
| | 22.05 | 2757.12 | 1.56 | | |
| NT-HF | 14.18 | 264.14 | 1.21 | 30.43 | 5.99 |
| | 16.14 | 435.80 | 1.23 | | |
| | 20.94 | 1332.04 | 5.35 | | |
| | 21.92 | 1914.64 | 1.41 | | |
| TR-HF | 14.54 | 510.00 | 1.19 | 59.38 | 6.08 |
| | 16.73 | 749.00 | 1.64 | | |
| | 20.53 | 1166.60 | 6.51 | | |
| | 21.78 | 2857.03 | 1.39 | | |
| NT-SF | 14.69 | 388.98 | 1.01 | 41.55 | 6.13 |
| | 16.42 | 422.53 | 1.14 | | |
| | 21.39 | 1558.34 | 6.11 | | |
| | 22.60 | 2666.32 | 1.38 | | |
| TR-SF | 14.91 | 972.00 | 1.52 | 71.76 | 6.26 |
| | 16.59 | 423.21 | 1.26 | | |
| | 20.18 | 1268.50 | 6.00 | | |
| | 22.40 | 4492.53 | 1.35 | | |
| NT-BF | 15.14 | 167.15 | 1.16 | 58.94 | 6.12 |
| | 16.55 | 149.96 | 1.05 | | |
| | 20.11 | 1120.49 | 5.69 | | |
| | 22.12 | 2729.25 | 1.38 | | |

(Continued)

**Table 3 (continued)**

| Fibers | $x_c$ (°) | H (a.u.) | FWHM (°) | CI (%) | L (nm) |
|---|---|---|---|---|---|
| TR-BF | 15.39 | 1162.28 | 1.21 | 75.51 | 6.55 |
| | 16.74 | 596.18 | 1.04 | | |
| | 20.40 | 1606.24 | 3.89 | | |
| | 22.16 | 6560.00 | 1.29 | | |

The ATR-FTIR technique was applied in order to identify the principal absorption bands for the functional groups present on the fibers. The results are presented in Figs. 7 and 8. Similar results were reported by Sahu et al. when analyzing the FTIR spectra of Rattan fibers subjected to different surface treatments [41]. From the results, it can be seen that the fibers treated with plasma exhibit the same functional groups as the untreated fibers. The bands located closest to 3334, 1160, and 897 $cm^{-1}$ are associated with hydroxyl (OH) groups, the stretching of the C-O bonds, and the stretching of the C-H bonds in the aromatic rings typical of cellulose, respectively. The bands located closest to 2920 and 1730 $cm^{-1}$ can be attributed to stretching of the C-H bonds in methyl (−CH3), methylene (−CH2), and C=O groups present in hemicellulose components. Additionally, the bands located at 1593, 1455, and 1423 $cm^{-1}$ may be related to the stretching of the C=C and C-H bonds in aromatic rings and aliphatic compounds of lignin. On the other hand, an increase in the intensities of the bands located at 3334, 2920, and 2155 $cm^{-1}$ can be observed in all the treated fibers. Similar results were obtained by Macedo et al. when they studied the effect of cold plasma treatment on the surface of Kapok fibers [42]. The increases in intensity at 3334 and 2920 $cm^{-1}$ suggest that the crystallinity of the fibers has improved, which can influence the interaction between infrared light and the fibers, causing an increase in transmittance in these absorption bands.

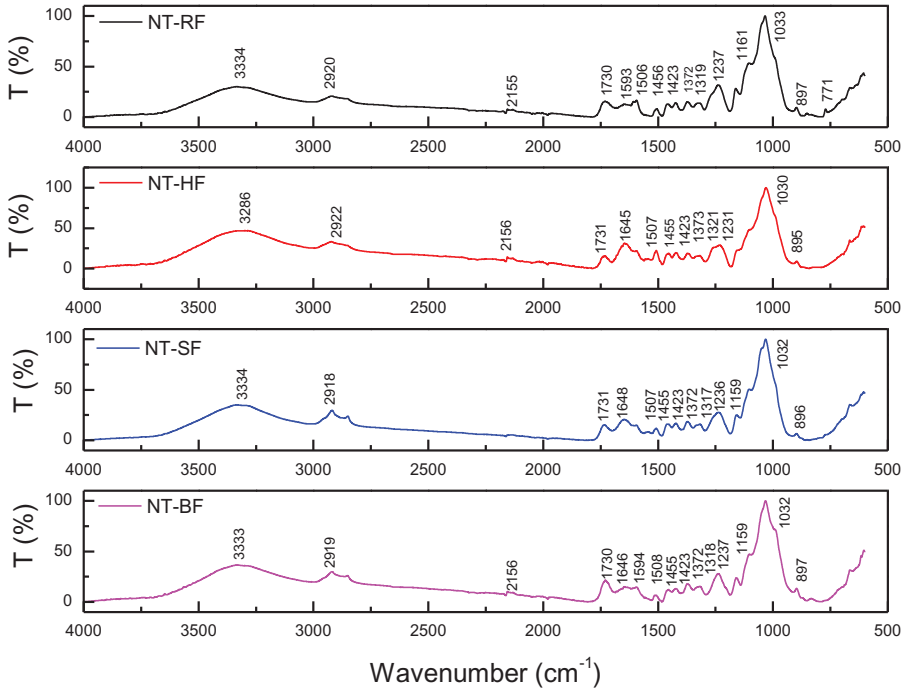


**Figure 7:** ATR-FTIR spectra for untreated fibers. T is the transmittance

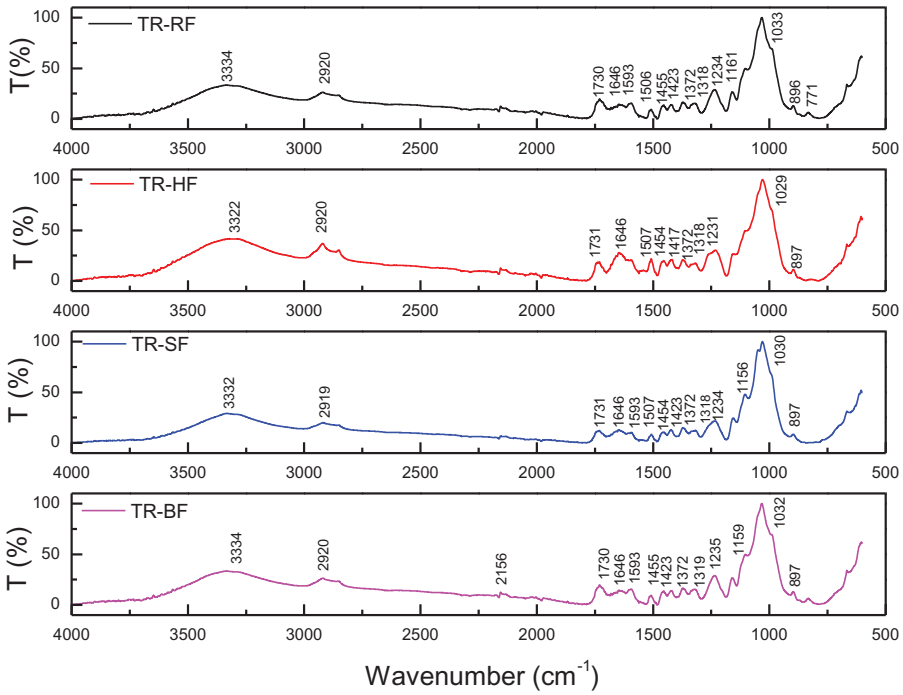


**Figure 8:** ATR-FTIR spectra for treated fibers. T is the transmittance

### *3.3 Effect of Treatment on the Physical and Mechanical Properties of the Vegetal Fibers*

The physical and mechanical properties of the vegetal fibers were determined, and the results are shown in Table 4. They show a reduction of between 14% and 18% in the D values of all the specimens. An increase of less than 30% in A can be observed in TR-RF and TR-HF fibers, while in TR-SF and TR-BF, this value increased to 50%. Additionally, because of the treatment, the Sw increased between 8% and 16% in all fibers. These changes are probably associated with the appearance of microvoids on the surface of the material due to the removal of impurities and non-cellulosic compounds during the treatment. On the other hand, a reduction of less than 20% in $\sigma_t$, $E_t$, and $\varepsilon$ values can be observed in the TR fibers. This decrease in the mechanical properties could be related both to the chemical modifications on the surface of the fibers and to the appearance of defects in the internal structure of the material, which can lead to the emergence of stress concentrations that affect the performance of the material when subjected to axial loads.

**Table 4:** Physical and mechanical properties of the fibers

| Fibers | d (mm) | D (kg/m$^3$) | A (%) | Sw (%) | $\sigma_t$ (MPa) | $E_t$ (GPa) | $\varepsilon$ (%) |
|---|---|---|---|---|---|---|---|
| NT-RF | 1.34 ± 0.03 | 390 ± 21 | 21.37 ± 0.23 | 11.62 ± 0.35 | 285 ± 18 | 2.81 ± 0.16 | 3.85 ± 0.11 |
| TR-RF | 1.27 ± 0.04 | 335 ± 13 | 26.34 ± 0.15 | 12.78 ± 0.26 | 234 ± 14 | 2.38 ± 0.11 | 3.25 ± 0.14 |
| NT-HF | 1.56 ± 0.05 | 600 ± 16 | 22.45 ± 0.21 | 14.59 ± 0.39 | 356 ± 12 | 3.75 ± 0.22 | 1.54 ± 0.24 |
| TR-HF | 1.44 ± 0.06 | 492 ± 12 | 28.92 ± 0.19 | 15.75 ± 0.62 | 301 ± 17 | 3.25 ± 0.34 | 1.28 ± 0.14 |
| NT-SF | 1.28 ± 0.04 | 470 ± 19 | 31.37 ± 0.32 | 11.94 ± 0.41 | 260 ± 13 | 2.33 ± 0.19 | 2.85 ± 0.15 |
| TR-SF | 1.23 ± 0.05 | 402 ± 11 | 46.41 ± 0.19 | 13.55 ± 0.34 | 213 ± 16 | 1.89 ± 0.22 | 2.55 ± 0.18 |
| NT-BF | 1.67 ± 0.08 | 660 ± 41 | 28.44 ± 0.26 | 14.59 ± 0.39 | 460 ± 11 | 3.21 ± 0.32 | 4.31 ± 0.19 |
| TR-BF | 1.55 ± 0.04 | 561 ± 18 | 43.25 ± 0.17 | 16.87 ± 0.33 | 385 ± 15 | 2.77 ± 0.26 | 3.55 ± 0.24 |

### *3.4 Physical and Mechanical Properties of Panels*

The physical properties of the panels were determined. The results are presented in Table 5.

**Table 5:** Physical properties of panels

| Panels | $D_w$ (kg/m$^3$) | D (kg/m$^3$) | A (%) | Sw (%) |
|---|---|---|---|---|
| NT-RF-P | 545 ± 14 | 689 ± 7 | 35.9 ± 3.5 | 25.9 ± 3.7 |
| TR-RF-P | 472 ± 21 | 638 ± 8 | 31.1 ± 2.9 | 16.6 ± 4.6 |
| NT-HF-P | 611 ± 17 | 735 ± 7 | 29.2 ± 2.2 | 22.1 ± 3.1 |
| TR-HF-P | 501 ± 9 | 658 ± 9 | 23.9 ± 1.9 | 16.5 ± 4.2 |
| NT-SF-P | 345 ± 6 | 551 ± 4 | 37.2 ± 4.3 | 29.1 ± 2.8 |
| TR-SF-P | 279 ± 13 | 503 ± 6 | 30.8 ± 3.6 | 21.3 ± 2.7 |
| NT-BF-P | 761 ± 15 | 840 ± 4 | 19.4 ± 2.8 | 16.6 ± 3.5 |
| TR-BF-P | 589 ± 8 | 720 ± 3 | 14.8 ± 2.0 | 13.3 ± 1.2 |

From the results presented in Table 5, a reduction of between 5% and 15% can be observed in the D of the panels made with treated fibers. The plasma treatment produced a significant effect on the physical properties of the panels. Furthermore, with the appearance of microvoids on the surface of the material, there was better penetration of the resin, which contributed to reducing the content of the voids available for absorbent liquids. The values of A and Sw were reduced by 10% and 35%, respectively. The panels made with treated fibers exhibited average Sw values of between 21.3% and 13.3%. These values are lower than the maximums established in the ISO 16894:2009(E) standard [43] for oriented strand boards (OSB) with a thickness greater than 5 mm used in dry conditions. Furthermore, the dimensional stability of TR-BF-P (Sw < 15%) suggests that they could be used as substitutes for conventional OSB in the construction of structural boards for use in humid conditions.

The absorption capacity of the panels made with treated fibers was compared with the maximum values established in EN 622 for medium-density fiberboards for use in dry and humid environments [44]. The results are presented in Table 6. On comparing the results, it is possible to see that the absorption capacity of the non-conventional panels varies between 14.80% and 31.1%. These values are lower than the maximum values established for commercial MDF panels [44].

**Table 6:** Comparison between absorption capacity of non-conventional panels and requirements for MDF exposed to different environmental conditions

| Panels | A (%) |
|---|---|
| TR-RF-P | 31.1 ± 2.9 |
| TR-HF-P | 23.9 ± 1.9 |
| TR-SF-P | 30.8 ± 3.6 |
| TR-BF-P | 14.8 ± 2.0 |
| MDF dry condition | <35 |
| MDF humid condition | <32 |

The mechanical properties of the panels subjected to axial loads was evaluated. The average basic tensile and compression stresses as a function of the unit strain are presented in Figs. 9 and 10. When analyzing the experimental results, an increase of between 15% and 50% in the tensile and compression strength of the panels reinforced with treated fibers can be observed. On the other hand, the selection of the reinforcement influenced the maximum strength of the specimens. TR-BF-P specimens exhibited the highest average strength values (41.6 MPa in tensile and 33.3 MPa in compression), while TR-SF-P exhibited the lowest values (15.22 and 10.8 MPa, respectively). Furthermore, an increase in stiffness in the elastic region and in toughness can be observed in all the panels made with the treated fibers. The maximum strength and the modulus of elasticity were determined by means of the numerical model developed using commercial finite-element software. Differences of less than 15% were found between the experimental and the numerical results, which are presented in Table 7. Similar results were obtained by Chen et al. [45] when they analyzed the mechanical behavior of conventional OSB panels subjected to axial loads.

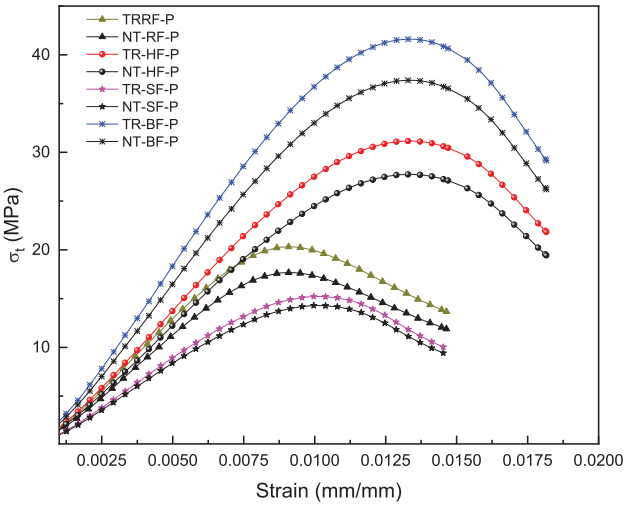


**Figure 9:** Tensile strength as a function of strain

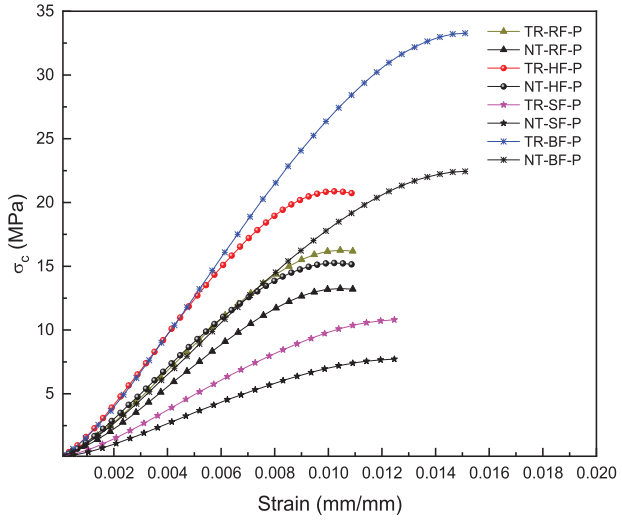


**Figure 10:** Compression strength as a function of strain

**Table 7:** Comparison between experimental and numerical results

| Panels | Tension parallel to surface | | | | Compression parallel to surface | | | |
|---|---|---|---|---|---|---|---|---|
| | $\sigma_{t(exp)}$ (MPa) | $\sigma_{t(num)}$ (MPa) | $E_{t(exp)}$ (MPa) | $E_{t(num)}$ (MPa) | $\sigma_{c(exp)}$ (MPa) | $\sigma_{c(num)}$ (MPa) | $E_{c(exp)}$ (MPa) | $E_{c(num)}$ (MPa) |
| NT-RF-P | 17.7 ± 2.1 | 18.67 | 2140 ± 16 | 2289 | 13.3 ± 1.2 | 14.76 | 1372 ± 17 | 1567 |
| TR-RF-P | 20.3 ± 3.6 | 21.39 | 2460 ± 21 | 2598 | 16.1 ± 1.8 | 17.85 | 1683 ± 11 | 1726 |
| NT-HF-P | 27.7 ± 4.5 | 29.21 | 2358 ± 34 | 2531 | 15.2 ± 2.8 | 16.06 | 1692 ± 14 | 1781 |
| TR-HF-P | 31.6 ± 2.7 | 33.56 | 2649 ± 21 | 2875 | 20.9 ± 3.4 | 23.62 | 2316 ± 27 | 2579 |
| NT-SF-P | 14.3 ± 2.3 | 15.64 | 1720 ± 13 | 1830 | 7.7 ± 1.1 | 8.64 | 667 ± 7 | 734 |
| TR-SF-P | 15.2 ± 2.9 | 16.13 | 1833 ± 17 | 1911 | 10.8 ± 1.9 | 11.67 | 929 ± 9 | 1045 |
| NT-BF-P | 37.4 ± 3.6 | 39.11 | 3014 ± 88 | 3290 | 22.4 ± 3.5 | 24.43 | 1684 ± 15 | 1752 |
| TR-BF-P | 41.6 ± 4.2 | 43.78 | 3353 ± 71 | 3569 | 33.3 ± 4.3 | 35.31 | 2499 ± 19 | 2678 |

The effect of the surface treatment on the experimental MOR and MOE values was determined by means of a three-point bending test. The graph of MOR *vs*. experimental displacement is shown in Fig. 11. An increase of between 10% and 18% for the bending strength of the panels made with plasma-treated fibers can be observed. The experimental results were compared with those obtained by the numerical simulations (see Table 8). TR-BF-P panels exhibited the highest MOR and MOE values (66.43 and 5304 MPa, respectively). On comparing the experimental results with those obtained with the numerical model, differences of less than 20% were found.

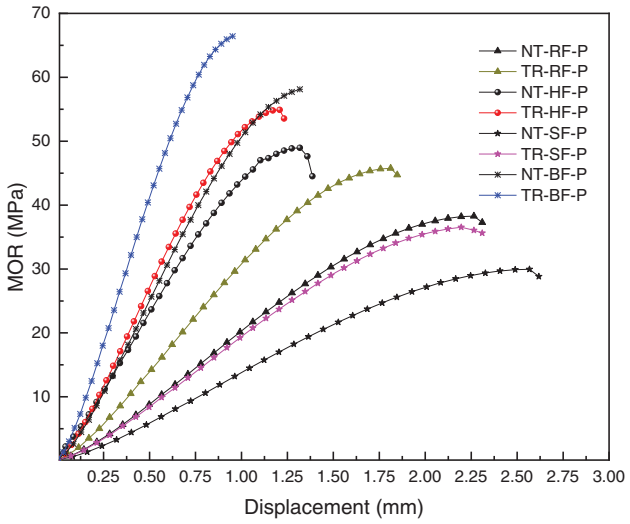


**Figure 11:** Results of bending tests: MOR, MPa

From the results presented in Figs. 9 to 11, the effect of the surface treatment with cold argon plasma on the performance of the specimens subjected to tension, compression, and static bending loads can be seen. Similar results were found by Raghavendra et al. when they analyzed the mechanical properties of hybrid composites made with bamboo-nettle-based plant fibers manufactured using the vacuum bag technique

[46]. The increase in the strength and the stiffness of all the panels could be associated with the increase of the adhesion in the interfacial region of the composite as a consequence of the partial removal of the lignin and other non-cellulosic compounds usually present in plant fibers. On the other hand, modifying the surface of the fibers increases their compatibility with the resin used as a matrix (in this case, castor oil), which contributes to improving the load transfer. Furthermore, it can be seen that the treatment slightly increased the deformation energy of the panels up to the breaking point.

**Table 8:** Comparison between experimental and numerical results

| Panels | $MOR_{(exp)}$ (MPa) | $MOR_{(num)}$ (MPa) | $MOE_{(exp)}$ (MPa) | $MOE_{(num)}$ (MPa) |
|---|---|---|---|---|
| NT-RF-P | 38.25 ± 1.91 | 43.99 | 1284 ± 90 | 1438 |
| TR-RF-P | 45.76 ± 3.20 | 51.25 | 1918 ± 115 | 2148 |
| NT-HF-P | 48.96 ± 2.94 | 57.77 | 2835 ± 255 | 3155 |
| TR-HF-P | 54.91 ± 2.75 | 62.05 | 3442 ± 275 | 3993 |
| NT-SF-P | 29.95 ± 1.20 | 26.66 | 884 ± 45 | 760 |
| TR-SF-P | 36.53 ± 2.56 | 30.32 | 1283 ± 73 | 1155 |
| NT-BF-P | 58.12 ± 4.65 | 63.93 | 3340 ± 134 | 3941 |
| TR-BF-P | 66.43 ± 3.89 | 77.06 | 5304 ± 186 | 6100 |

The bending properties (MOR and MOE) of the treated panels was compared with the minimum requirements established in EN 310 for the use of the medium-density fiberboards (MDF) in dry and humid conditions [47]. The results are presented in Table 9. From the results, it can be seen that the panels made with plasma-treated plant fibers have resistance values between 36.53 and 66.43 MPa. These values exceed by more than 60% the minimum values established for commercial MDF boards for general use (22 MPa in dry environments and 26 MPa in humid environments). Analyzing the flexural elasticity modulus, it can be seen that the TR-HF-P and TR-BF-P panels exhibit MOE values greater than 2500 MPa (3442 and 5304 MPa, respectively). These results show the viability of its use as a substitute for commercial MDF boards in those applications in which the material must guarantee good resistance and rigidity, such as interior and exterior wall coverings. On the other hand, it can be seen that although the TR-RF-P and TR-SF-P panels have high MOR values (45.76 and 36.53, respectively), the elastic modulus values are lower than the minimum specified in EN 310, which could be a limitation for its use in applications that require restricting the deformations that occur in the structure [47].

**Table 9:** Comparison between static bending properties of non-conventional panels and requirements for MDF exposed to different environmental conditions

| Panels | MOR (MPa) | MOE (MPa) |
|---|---|---|
| TR-RF-P | 45.76 ± 3.20 | 1918 ± 115 |
| TR-HF-P | 54.91 ± 2.75 | 3442 ± 275 |
| TR-SF-P | 36.53 ± 2.56 | 1283 ± 73 |
| TR-BF-P | 66.43 ± 3.89 | 5304 ± 186 |
| $MDF_{dry\ conditions}$ | >22.00 | >2200 |
| $MDF_{humid\ conditions}$ | >26.00 | >2500 |

Fig. 12 shows the variation of the load with the vertical displacement of the load cell during the buckling test. The critical buckling load was identified as the first point on the graph at which the load remained almost constant for increasing displacements once the elastic deformation phase had been exceeded. Pcr values of between 2490 and 6330 N for the panels made with untreated fibers were observed, while the panels made with treated fibers exhibited an increase of up to 60% in the Pcr values. The NT-SF-P panels exhibited lateral instability for lower load values, and the TR-BF-P ones exhibited higher buckling strength. An increase in load after the structure has entered the buckling state can be observed for all the panels, being more visible in NT-BF-P and TR-BF-P. This behavior may indicate that a part of the deformations that occur during the buckling of the panels is of elastic origin, and for that reason they are recoverable. However, other factors, such as the redistributions of the loads and the support conditions used, can affect the mechanical response of the material in the post-buckling stage [48]. A numerical model was implemented in order to obtain the numerical values of the critical buckling load for the first mode of linear buckling. A comparison between the experimental and the numerical Pcrvalues is presented in Table 10. Differences between the experimental results and those obtained with the numerical model were lower than 15%.

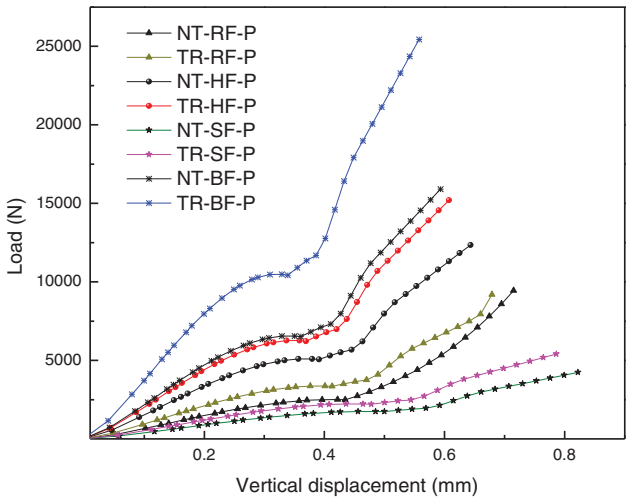


**Figure 12:** Experimental critical buckling load as a function of vertical displacement

**Table 10:** Comparison between experimental and numerical results

| Panels | $Pcr_{(exp)}$ (MPa) | $Pcr_{(num)}$ (MPa) |
|---|---|---|
| NT-RF-P | 2490 ± 249 | 2762 |
| TR-RF-P | 3380 ± 213 | 3671 |
| NT-HF-P | 4930 ± 346 | 5167 |
| TR-HF-P | 6070 ± 379 | 6319 |
| NT-SF-P | 1690 ± 151 | 1932 |
| TR-SF-P | 2150 ± 178 | 2431 |
| NT-BF-P | 6330 ± 418 | 6011 |
| TR-BF-P | 10,100 ± 501 | 9532 |

## 4 Conclusions

Due to their biodegradable nature and their physical and mechanical properties, the use of plant fibers as substitutes for synthetic fibers in the manufacture of alternative composite materials has gained interest in recent years. Non-conventional panels present advantages associated with environmental sustainability, reduction of greenhouse gases, light weight, and high resistance and rigidity under mechanical loads.

In this paper, fibers obtained from four plant species native to South America were used. The rapid growth and wide availability of the species used allow the development of a biodegradable and sustainable material. However, the efficient use of this type of fiber requires deepening the understanding of both the effect of the treatments that are applied to their surface and of the mechanical performance of the compounds in which they act as reinforcement.

The surface of the fibers was treated with cold argon plasma. With this treatment, the generation of chemical waste usually seen with traditional treatment methods, such as mercerization, is reduced. The effect of treatment with cold argon plasma on the physical and mechanical properties of vegetable fibers was analyzed. From the results, it can be concluded that the treatment with cold argon plasma significantly affected the structure and the chemical properties of the fibers. The increase in the O/C ratio of vegetal fibers, the crystallinity index, and the of length of the crystallites may be associated with the oxidation of their surface. On the other hand, no significant changes were observed in the characteristic absorption bands of the main functional groups. This could be associated with a combination of factors, such as the depth of plasma penetration, the stability of the functional groups, and the specific treatment conditions.

Another aspect to consider is the appearance of micro voids as a result of the surface treatment. The results show that increasing the porosity of the fibers increases their capacity to retain liquids and reduces their density. Although this may represent a negative aspect, once the material is used as a reinforcement of a biopolymeric matrix, it is possible to increase the penetration of the resin, which contributes to improving the fiber-matrix interface and reducing the absorption capacity of the biocomposites. At the same time, the reduction in the density of the fibers favors the production of lighter composites, which allows reducing the self-weight in structural applications.

Despite the reduction in the strength and stiffness of the fibers, an increase in the mechanical performance of the panels was observed. The removal of non-cellulosic compounds and some impurities adhered to the surface of the fibers increased the adhesion between the fibers and the castor oil resin, improving the transfer of loads and, therefore, the strength and stiffness of the panels.

Understanding the mechanical behavior of biocomposites subjected to different loading conditions is important for assuring the safety of their use in different engineering applications. An analysis of the stresses and deformations that occur in the material when it is subjected to different loading conditions contributes to establishing selection criteria in accordance with its possible use. The physical and mechanical properties of TR-RF-P, TR-HF-P, and TR-SF-P encourage their use as a substitute for MDF panels, OSB boards, and other conventional composites frequently used as non-structural interior panels (in partition walls, floors, and non-load-bearing prefabricated elements). The strength, stiffness, and dimensional stability of TR-BF-P are compatible with the minimum value requirements for the use of MDF, and OSB for structural purposes in humid conditions. However, the evaluation of the physical and mechanical properties of the material must be complemented with an economic feasibility study that allows evaluating the costs of using the material on a large scale.

Finally, the development of numerical models that validate the experimental results with an acceptable level of reliability is an important tool that allows predicting the behavior of the material, thus optimizing the design and manufacturing processes.

**Acknowledgement:** The authors gratefully acknowledge Vicerrectoría de Investigaciones at the Universidad Militar Nueva Granada (UMNG, Colombia) for financing the research.

**Funding Statement:** This paper is a derivative product of the project INV-ING-3188 financed by the Vicerectory of Research of Universidad Militar Nueva Granada.

**Author Contributions:** The authors confirm the contributions to the paper as follows: study concept and design: Martha L. Sánchez; data collection: Martha L. Sánchez, G. Capote; analysis and interpretation of results: Martha L. Sánchez, G. Capote; draft manuscript preparation: Martha L. Sánchez, G. Capote. All authors reviewed the results and approved the final version of the manuscript.

**Availability of Data and Materials:** All data are available in the manuscript.

**Ethics Approval:** Not applicable.

**Conflicts of Interest:** The authors declare that they have no conflicts of interest to report regarding the present study.

## References

1. Barbhuiya S, Das BB. Life cycle assessment of construction materials: methodologies, applications and future directions for sustainable decision-making. Case Stud Constr Mater. 2023;19(7):1–8. doi:10.1016/j.cscm.2023.e02326.
2. Gruber E. Beyond carbon in socioenvironmental assessment: life cycle assessment as a decision support tool for net-zero energy systems. Energy Clim Change. 2021;2:100061. doi:10.1016/j.egycc.2021.100061.
3. Zimmer A, Bachmann SAL. Challenges for recycling medium-density fiberboard (MDF). Results Eng. 2023;19:101277. doi:10.1016/j.rineng.2023.101277.
4. Tenorio-Alfonso A, Sanchez MC, Franco JM. Impact of the processing method on the properties of castor oil/cellulose acetate polyurethane adhesives for bonding wood. Int J Adhes Adhes. 2022;116:103153. doi:10.1016/j.ijadhadh.2022.103153.
5. Chen T, Wu Y, Qiu J, Fei M, Qiu R, Liu W. Interfacial compatibilization via *in-situ* polymerization of epoxidized soybean oil for bamboo fibers reinforced poly(lactic acid) biocomposites. Compos Part A Appl Sci Manuf. 2020;138(3):106066. doi:10.1016/j.compositesa.2020.106066.
6. Awad SA, Jawaid M, Ismail AS, Khalaf EM, Abu-Jdayil B. Dimension stability, tensile and thermomechanical properties of bamboo/oil palm fibre reinforced bio-epoxy hybrid biocomposites. J Mater Res Technol. 2024;30:7440–6. doi:10.1016/j.jmrt.2024.05.130.
7. Nazari M, Jebrane M, Terziev N. New hybrid bio-composite based on epoxidized linseed oil and wood particles hosting ethyl palmitate for energy storage in buildings. Energy. 2023;278(9):127692. doi:10.1016/j.energy.2023.127692.
8. Mir M, Wilson MD. Flax fiber-chitosan biocomposites with tailored structure and switchable physicochemical properties. Carbohydr Polym Technol Appl. 2023;6(1):100397. doi:10.1016/j.carpta.2023.100397.
9. Moyo M, Kanny K, Velmurugan R. Performance of kenaf non-woven Mat/PLA biocomposites under medium velocity impact. Fibers Polym. 2020;21(11):2642–51. doi:10.1007/s12221-020-1130-z.
10. Torres S, Ortega R, Acosta P, Calderón E. Hot incremental forming of biocomposites developed from linen fibres and a thermoplastic matrix. J Mech Eng. 2021;77(3):127–32. doi:10.5545/sv-jme.2020.6936.
11. Gallala W, Khater H, Souilah M, Nouri K, Ben Regaya M, Gaied M. Production of low-cost biocomposite made of palm fibers waste and gypsum plaster. Rev Int Contam Ambie. 2020;36(2):475–83. doi:10.20937/RICA.53541.
12. Kamaruddin Z, Jumaidin R, Ilyas R, Selamat M, Alamjuri R, Md Yusof F. Biocomposite of cassava starch-cymbopogan citratus fibre: mechanical, thermal and biodegradation properties. Polymers. 2022;14(3):514:1–19. doi:10.3390/polym14030514.

13. Manu T, Nazmi AR, Shahri B, Emerson N, Huber T. Biocomposites: a review of materials and perception. Mater Today Commun. 2022;31(10):103308. doi:10.1016/j.mtcomm.2022.103308.
14. Gondaliya A, Alipoormazandarani N, Kleiman M, Foster EJ. Sustainable compressed biocomposite: review on development and novel approaches. J Clean Prod. 2023;35(4):105846. doi:10.1016/j.mtcomm.2023.105846.
15. Gowda TGY, Vinod A, Madhu P, Rangappa SM, Siengchin M, Jawaid M. Mechanical and thermal properties of flax/carbon/kevlar based epoxy hybrid composites. Polym Comp. 2022;43(8):5649–62. doi:10.1002/pc.26880.
16. Vinod A, Tengsuthiwat J, Gowda Y, Vijay R, Sanjay MR. Jute/Hemp bio-epoxy hybrid bio-composites: influence of stacking sequence on adhesion of fiber-matrix. Int J Adhes Adhes. 2022;113:103050. doi:10.1016/j.ijadhadh.2021.103050.
17. Gowda TGY, Vinod A, Madhu P, Vinod K, Sanjay MR, Siengchin S. Dhakal HN. A new study on flax-basalt-carbon fiber reinforced epoxy/bioepoxy hybrid composites. Polym Compos. 2021;42(4):1891–900. doi:10.1002/pc.25944.
18. Vinod A, Sanjay MR, Suchart S, Jyotishkumar P. Renewable and sustainable biobased materials: an assessment on biofibers, biofilms, biopolymers and biocomposites. Clean Prod. 2020;258:120978. doi:10.1016/j.jclepro.2020.120978.
19. Teraube O, Agopian JC, Dubois M. Surface modification of sized vegetal fibers through direct fluorination for eco-composites. J Fluorine Chem. 2020;238:109618. doi:10.1016/j.jfluchem.2020.109618.
20. Chen Z, Du K, Yin H, Zhang D, Gao J, Song W, et al. Surface modification of bamboo fiber with dopamine associated by laccase for poly(3-hydroxylbutyrate) biocomposites. J Clean Prod. 2023;389(21):135996. doi:10.1016/j.jclepro.2023.135996.
21. Wu M, Jia L, Lu S, Qin Z, Wei S, Yan R. Interfacial performance of high-performance fiber-reinforced composites improved by cold plasma treatment: a review. Surf Interfaces. 2021;24(1):101077. doi:10.1016/j.surfin.2021.101077.
22. Sánchez ML, Patiño W, Cárdenas J. Physical-mechanical properties of bamboo fibers-reinforced biocomposites: influence of surface treatment of fibers. J Build Eng. 2020;28(6):101058. doi:10.1016/j.jobe.2019.101058.
23. Sánchez ML, Capote G, Patiño JP. Effect of surface treatment of fibers on the accelerated aging of biocomposites. Constr Build Mater. 2021;271(17):121875. doi:10.1016/j.conbuildmat.2020.121875.
24. Mary SK, Thomas MS, Koshy RR, Pillai PKS, Pothan LA, Thomas S. 11 Adhesion in biocomposites: a critical review. In: Progress in adhesion and adhesives. Publishing LLC; 2021. vol. 6, p. 531–57. doi:10.1002/9781119846703.ch11.
25. Pathak DK, Purohit R, Soni A, Gupta HS. Buckling analysis of composite laminated plate in different boundary conditions under thermo mechanical loading. Mater Today Proc. 2020;44(1):2211–4. doi:10.1016/j.matpr.2020.12.355.
26. Jiao-Wang L, Larriba C, Santiuste C. On the experimental validation of Ludwick law to predict critical buckling load of nonlinear elastic columns. Compos Struct. 2022;303(10):116237. doi:10.1016/j.compstruct.2022.116237.
27. Gioffrè M, Pepi C. Environmental aging effects on mechanical behavior of an hemp based biocomposite material for structural strengthening. J Build Eng. 2024;91(23):109571. doi:10.1016/j.jobe.2024.109571.
28. Jungstedt E, Oliaei E, Li L, Östlund S, Berglund L. Mechanical behavior of all-lignocellulose composites—comparing micro-and nanoscale fibers using strain field data and FEM updating. Compos Part A Appl Sci Manuf. 2022;161:107095. doi:10.1016/j.compositesa.2022.107095.
29. Kan Y, Li J, Zhang S, Gao Z. Novel bridge assistance strategy for tailoring crosslinking networks within soybean-meal-based biocomposites to balance mechanical and biodegradation properties. J Chem Eng. 2023;472(2):144858. doi:10.1016/j.cej.2023.144858.
30. ASTM International. Standard test method for alpha-cellulose in wood. ASTM D1103-21. West Conshohocken, PA: ASTM International; 2021.
31. ASTM International. Standard test methods for water solubility of wood. ASTM D1110-21. West Conshohocken, PA: ASTM International; 2021.
32. ASTM International. Standard test method for acid-insoluble lignin in wood. ASTM D1106-21. West Conshohocken, PA: ASTM International; 2021.

33. Nam S, French AD, Condon BD, Concha M. Segal crystallinity index revisited by the simulation of X-ray diffraction patterns of cotton cellulose I and cellulose II. Carbohydr Polym. 2016;135(4633):1–9. doi:10.1016/j.carbpol.2015.08.035.
34. ASTM International. Standard test methods for density and specific gravity (relative density) of plastics by displacement. ASTM D792-20. West Conshohocken, PA: ASTM International; 2020.
35. ASTM International. Standard test method for density of high-modulus fibers. ASTM D3800-20. West Conshohocken, PA: ASTM International; 2020.
36. Dumont P, Martoïa F, Orgéas L. 11. Compression moulding. In: Design and manufacture of structural composites. Woodhead Publishing Series in Composites Science and Engineering. Elsevier Ltd.; 2022. p. 273–300. doi:10.1016/B978-0-12-819160-6.00018-4.
37. ASTM International. Standard test methods for density and specific gravity (relative density) of wood and wood-based materials. ASTM D2395-17. West Conshohocken, PA: ASTM International; 2017.
38. ASTM International. Standard test methods for evaluating properties of wood-base fiber and particle panel materials. ASTM D1037-20. West Conshohocken, PA: ASTM International; 2020.
39. Sawangrat C, Thipchai P, Kaewapai K, Jantanasakulwong K, Suhr J, Wattanachai P, et al. Surface modification and mechanical properties improvement of bamboo fibers using dielectric barrier discharge plasma treatment. Polymers. 2023;15(7):1711. doi:10.3390/polym15071711.
40. Vinod A, Rangappa S, Srisuk R, Tengsuthiwat J, Ramnath A, Siengchin S. Agro-waste Capsicum Annum stem: an alternative raw material for lightweight composites. Ind Crops Prod. 2023;193:116141. doi:10.1016/j.indcrop.2022.116141.
41. Sahu S, Sahu SBPBP, Roul MK. Influence of various surface treatments on mechanical, thermal, morphological, and water absorption properties of rattan (*Calamus beccarii*) fiber. J Nat Fibers. 2023;20(1):2125924. doi:10.1080/15440478.2022.
42. Macedo M, Silva G, Feitor M, Costa T, Ito E, Melo J. Surface modification of kapok fibers by cold plasma surface treatment. J Mater Res Technol. 2020;9(2):2467–76. doi:10.1016/j.jmrt.2019.12.077.
43. ISO. Wood-based panels—oriented strand board (OSB)—definitions, classification and specifications; 2009. ISO 16894:2009.
44. European Committee for Standardization. European standard. BS EN 622. Wood-based panels-specifications-part 5: requirements for dry process MDF. 2021. doi:10.3403/BSEN622.
45. Chen G, He B. Stress-strain constitutive relation of OSB under axial loading: an experimental investigation. BioResources. 2017;12(3):6142–56. doi:10.15376/biores.12.3.6142-6156.
46. Raghavendra BS, Thyagara NR, Shreyas PS. Effect of surface treatment on tensile and buckling characteristics of natural fibre-based hybrid composites. Mater Today Commun. 2022;54(2):147–51. doi:10.1016/j.matpr.2021.08.198.
47. European Committee for Standardization. European standard. BS EN 310. Wood-based panels-determination of modulus of elasticity in bending and bending strength. 2019. doi:10.3403/00299457U.
48. Eslami MR. Chapter 2 buckling and post-buckling of beams. In: Buckling and post buckling of beams, plates, and shells. Cham, Switzerland: Springer International Publishing; 2018. p. 7–97. doi:10.1007/978-3-319-62368-9.